Computational and Structural Biotechnology Journal 18 (2020) 1625–1638

COMPUTATIONAL AND STRUCTURAL BIOTECHNOLOGY JOURNAL

journal homepage: www.elsevier.com/locate/csbj

Exploring the structural basis of conformational heterogeneity and autoinhibition of human cGMP-specific protein kinase Iα through computational modelling and molecular dynamics simulations

Arooma Maryam [a,b,c], Rana Rehan Khalid [a,1], Sundeep Chaitanya Vedithi [b,1], Abdulilah ECE [c], Suleyman Selim Çınaroğlu [d], Abdul Rauf Siddiqi [a,*], Tom L. Blundell [b,*]

[a] Department of Biosciences, COMSATS University Islamabad (CUI), Park Road, Islamabad 4550, Pakistan
[b] Department of Biochemistry, University of Cambridge, 80 Tennis Court Rd., Cambridge CB2 1GA, UK
[c] Department of Pharmaceutical Chemistry, Faculty of Pharmacy, Biruni University, Istanbul 34010, Turkey
[d] Department of Biochemistry, University of Oxford, South Parks Road, Oxford OX1 3QU, UK

ARTICLE INFO

Article history:
Received 24 February 2020
Received in revised form 5 June 2020
Accepted 6 June 2020
Available online 12 June 2020

Keywords:
Cyclic guanosine monophosphate (cGMP)
Protein kinase Iα (PKGIα)
Auto-inhibitory domain (AI)
Cyclic Nucleotide binding domain-A (CNB-A)

ABSTRACT

Protein kinase Iα (PKGIα) is a pivotal cyclic guanosine monophosphate (cGMP) signalling protein. Major steps related to the structural plasticity of PKGIα have been inferred but the structural aspects of the auto-inhibition and multidomain tertiary organization of human PKGIα in active and inactive form are not clear. Here we combine computational comparative modelling, protein–protein docking and molecular dynamics (MD) simulations to investigate structural details of the repressed state of the catalytic domain of PKGIα. Exploration of the potential inhibitory conformation of the auto-inhibitory domain (AI) within the catalytic cleft reveals that the pseudo-substrate motif binds with residues of the glycine rich loop and substrate-binding lobe. Dynamic changes as a result of coupling of the catalytic and AI domains are also investigated. The three-dimensional homodimeric models of PKGIα in the active and inactive state indicate that PKGIα in its inactive-state attains a compact globular structure where cyclic nucleotide binding (CNB-A/B) domains are buried, whereas the catalytic domains are inaccessible with their substrate-binding pockets facing the N-terminal of CNB-A. Contrary to this, the active-state model of PKGIα shows an extended conformation where CNB-A/B domains are slightly rearranged and the catalytic domains of homodimer flanking the C-terminal with their substrate binding lobes free to entrap downstream proteins. These findings are consistent with previously reported static images of the multidomain organization of PKGIα. Structural insights pertaining to the conformational heterogeneity and auto-inhibition of PKGIα provided in this study may help to understand the dynamics-driven effective regulation of PKGIα.

1. Background

Cyclic guanosine monophosphate (cGMP) specific protein kinase (PKG), a core regulator of the cGMP signalling pathway, displays a kinase-specific conformational heterogeneity at the structural level. In mammals, PKG has three isoforms, namely PKGIα, PKGIβ and PKGII, which share an almost identical domain configuration [1,2]. Like other eukaryotic kinases, cGMP specific protein kinases (PKGs) behave as dynamic switches; they exist in a compact ball-like folded form in their native cGMP-free inactive functional state but adopt a strikingly different and distinct cGMP-dependent extended conformation in the active functional state [2,3]. The consequences of cGMP binding to PKGI at a structural level have been a focus of investigation for more than 40 years and much is now understood at the single- or double-domain level. However, the quest to solve the structures of the full-length, multidomain structural assemblies of the two key functional states (inhibited and catalytically active) of human PKGs is still in progress [4,5].

Each PKG polypeptide is divided into two regions: a regulatory (R) region and a catalytic (C) region. The regulatory region is composed of four functional domains [1]. At the N-terminus, a coiled-coil leucine zipper is present, which is important for the homod-

* Corresponding authors.
E-mail addresses: araufsiddiqi@comsats.edu.pk (A.R. Siddiqi), tlb20@cam.ac.uk (T.L. Blundell).
[1] Rana Rehan Khalid and Sundeep Chaitanya contributed equally to this work.

https://doi.org/10.1016/j.csbj.2020.06.016
2001-0370/

imerization and subcellular localization of the PKGs. Following the leucine zipper domain is an auto-inhibitory (AI) domain, which engages the catalytic region of the PKG in the committed/inactive state. Next to the AI domain, there are two tandemly arranged low and high affinity cGMP binding domains (CNB-A & CNB-B) [2]. The C-terminal catalytic region of PKG, depicted in Fig. 1A, is further subdivided into two sub-domains: the kinase sub-domain where the Mg^{2+}/ATP binds and the AGC-kinase C-terminal domain where substrate/downstream proteins bind and phosphorylation occurs [6].

High-resolution protein structures determined by X-ray crystallography and NMR techniques have provided a wealth of structural information on the isolated domains of PKGIα and PKGIβ. Crystal structures of the individual leucine zipper domain (PDB Id: 4R4L) and cyclic nucleotide-binding domains (CNB-A and CNB-B) (PDB Id: 4Z07) in the dimeric state have revealed the molecular details of the cGMP-dependent conformational change leading to the activation and dimerization of PKGIα. In addition to this, the catalytic domain has been solved in both the apo-form (PDB Id: 6BDL) and the ligand-bound form (PDB Id: 6C0T) [7,8], but the structural basis of the auto-inhibitory mechanism in PKGIα is still obscure and needs to be addressed as part of understanding the structural assembly of the inactive human PKGIα.

cGMP protein kinases including PKGIα, PKGIβ and PKGII possess an AI domain at the N-terminal regulatory region that carries an inhibitory motif called the "pseudo-substrate" motif to regulate the activation of catalytic domain [10,11]. Consistent with the highly conserved function of the auto-inhibitory mechanism present in eukaryotic protein kinases, previous studies have identified conserved residues of the substrate-like motif of the AI domain [12–15]. However, how the AI domain engages the catalytic cleft in the inactive state is not understood. Which residues and what kind of molecular interactions stabilize the inhibited state of the catalytic domain need further investigation, as do the existence of any conformational changes within the catalytic domain to accommodate the AI domain. In this investigation, we focus on the study of the conformation of the AI domain with the potential to inhibit the activity of human PKGIα when complexed with the catalytic domain.

The proteins central to the human cGMP signalling pathway are complex, large multi-domains structures. Despite the improvement in experimental methods of protein structure determination, there are still limitations in defining the assembly of human multi-domain protein complexes [16]. Recent studies have explored how to leverage and integrate the computational structure-prediction techniques with already known experimental data of the protein fragments for the holistic determination of the quaternary structures and dynamics of human multi-domain proteins [17–19].

In the case of PKGIα, hypothetical models of inactive and active conformations of human PKGIα have been proposed based on the aforementioned structural data of standalone domains of PKGIβ and closely related homologous structures of cyclic adenosine monophosphate kinase (PKA) [9,20]. The inactive and active state models given in Fig. 1B portray the relative orientations of adjacent domains that govern the quaternary packing of PKGI homodimer in both functional states [9]. These models serve nicely as the starting point for computational assembly and prediction of a comprehensive multicomponent structure of PKGI-α in catalytically committed (active) as well as uncommitted (inactive) states.

To model the inactive PKGIα, it is crucial to understand the structural details of the association of AI and catalytic domains while in the inactive state. The lack of availability of the structure of the AI domain and its low (<20%) sequence identity with other known proteins make it extremely challenging to delineate the functional relationship of the AI domain to the auto-inhibitory mechanism of PKGIα.

In the present study, we explore the spatial orientation/ binding mode of the AI domain within the PKGIα catalytic domain as well as the nature of the molecular interactions between the AI-catalytic domain complex using a protein-structure modelling approach coupled with protein–protein docking and molecular dynamics (MD) simulations. In the first step, the three dimensional (3D) computational protein model was predicted and then docked into the catalytic domain to probe the near-native repressed state of the PKGIα catalytic domain. Multiple docked conformations of the AI-catalytic domain complex were evaluated through MD simulations to map out the approximate binding mode and resultant conformational transitions of the restrained state of the catalytic domain that occur in response to the binding of AI domain inside the catalytic cleft.

The present study was further extended to the full-length structure prediction of the PKGIα in both key states to map the conformational diversity of PKGIα in the cGMP signalling pathway.

2. Materials and methods

2.1. Structure prediction of auto-inhibitory subdomain through threading

Determining the structure of the AI domain is the cornerstone to understanding the molecular organisation, autoinhibitory mechanism and activation of the full length PKGIα. In PKGIα, there is no experimentally solved structure for the region spanning amino acids 47 to 102. This sequence region covering 25 functionally important amino acids of the AI domain binds and inactivates the catalytic region through the pseudo-substrate motif, to down-regulate the activity of PKGIα. To define the structure of the AI domain, the amino acid sequence of the query structure was retrieved from UniProt (Uniprot ID: **Q13976**) [21] and a PSI-BLAST search was performed against the Protein Data Bank (PDB) templates [22,23]. All the templates identified in the BLAST search were < 20% in sequence identity to the query sequence. In the absence of an appropriate template, a threading technique was employed for 3D structure prediction. The AI domain accounts for 25 residues which was too short for the structure prediction on I-TASSER suite [24] hence, the sequence length was extended to 55 amino acids. This was done to reduce false positivity in the results and achieve a good quality model. I-TASSER identified the 10 best templates by using LOMETs and generated multiple template sequence alignments using a number of threading programs. The initial model was selected based on TMalign [25] and C-score [26]. Model refinement was performed in UCSF Chimera [27] and evaluation of the refined model was achieved using RAMPAGE and MolProbity [28].

2.2. Protein–protein docking of catalytic & auto-inhibitory domain

Past studies reported that the N-terminal AI domain takes hold of the C-terminal catalytic domain in the PKGIα inactive state. Interaction of the two oppositely located domains induces a compact ball-like folded state. There is no homologous template available to aid in the prediction of the proposed inhibited/ committed conformation of the catalytic and AI domains. To investigate the correct orientation as well as the role of the AI domain in the repressed state of PKGIα, a predicted model of the AI domain was docked inside the active cleft of the catalytic pocket (PDB Id:6C0T) [7] using three different protein–protein docking programs, i.e. DOCK module of ClusPro [29], GRAMMX server [30] and pyDock [31]. A few biochemical studies report the composition of the pseudo-substrate motif of the AI domain based on the evolutionary conservation with its closely related homologous region

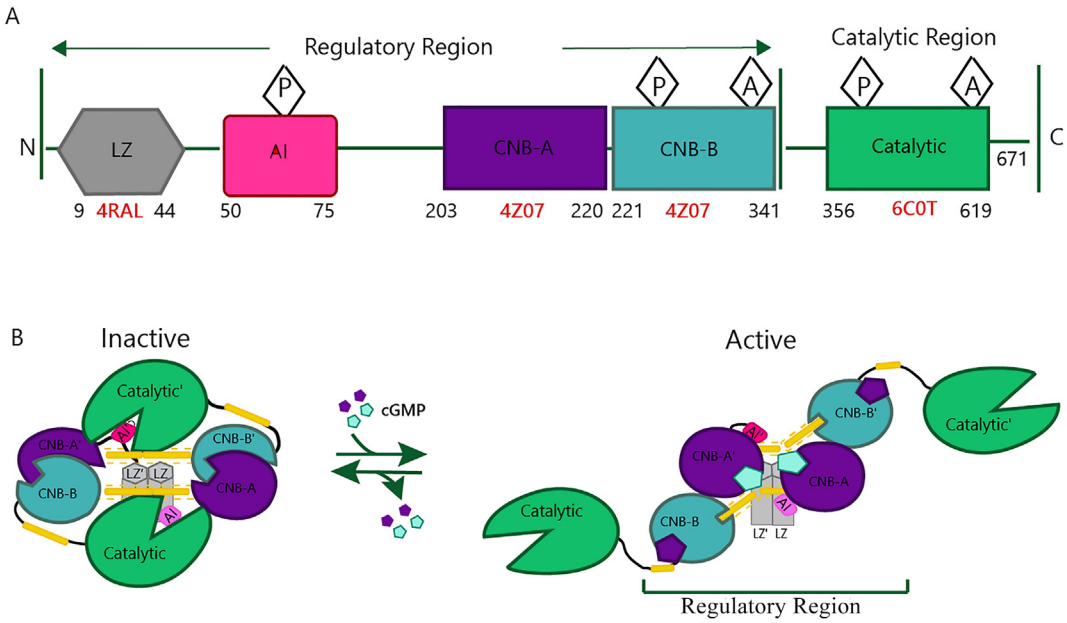

Fig. 1. A) The domain architecture of PKGIα. PKGIα is divided into regulatory and catalytic regions. The regulatory region comprises a leucine zipper domain (grey), auto-inhibitory domain (AI) (magenta), cGMP high affinity binding domain (purple) and cGMP low affinity binding domain (cyan). At the C-terminus, the catalytic domain is present and highlighted in green colour. Domain boundaries and PDB IDs of structurally solved domains are given below. Phosphorylation and acetylation sites of the respective domains are also highlighted. B) Models illustrating how human PKGIα folds in its inactive and active conformations (9). (For interpretation of the references to colour in this figure legend, the reader is referred to the web version of this article.)

in cAMP protein kinase (PKA) and other homologues [12,32,33]. In pyDock and ClusPro, restraints describing known residues of the AI domain were defined for their preferential docking within the catalytic cleft. At first multiple top ranked docked complexes were subjected to two-dimensional (2D) interaction analysis using Ligplot^{+} to screen the best docked poses with potential interactions between catalytic domain residues and already known pseudo-substrate residues of the AI domain. These complexes were then further selected for three-dimensional (3D) interaction analysis where four out of the six residues of the pseudo-substrate motif (RAQGISA) were interacting with the catalytic domain. Shape complementarity according to the proposed inactive conformation was also an additional criterion for the selection of potential docked poses. A comprehensive three-dimensional (3D) interaction analysis was performed in Intermezzo (Ochoa Montano B, Blundell TL, unpublished) to confirm the nature of intermolecular interactions in our selected docked complexes. The Intermezzo generated interaction analysis was refined in PyMol [34]. To investigate the potential binding pocket and/or catalytic residues of the PKGIα catalytic domain, hotspot analysis and ligand-interaction analysis of the co-crystal structure of PKGIα catalytic domain (PDB Id: 6C0T) were also performed using the Fragment Hotspots web application [35] and Ligplot^{+} tool. These analyses helped us to identify the catalytic residues and active site groove of the catalytic domain so that the occupancy of secondary structural elements of the catalytic pocket by the residues of the AI domain can be observed. Docking energy, inhibitory conformation and maximum number of inter-domain molecular interactions were used to choose three best complexes.

2.3. Molecular dynamics simulations

Of the three top ranked structures, AI2 and AI3 were selected for molecular dynamics (MD) simulations due to the higher number of hydrogen-bond interactions and occupancy of phosphorylation sites in the inhibited state. All atom MD simulations were performed through Amber14 [36]. The apo-form of the catalytic domain of PKGIα (PDB Id: 6BDL) was also used for MD simulations. The correct protonation states of the ionizable amino acids in our selected complexes were identified through UCSF Chimera PDB2PQR tool [27] using the AMBER (ff14SB) force-field [37]. Solvation of all the protein complexes under study was achieved using a rectangular box of TIP3P water molecules [38]. TIP3P water was extended 12 Å from solute atoms in all dimensions afterwards, and systems were neutralized using sodium (Na^{+}) and chloride (Cl^{-}) ions. All receptor structures were parameterized using AMBER FF99SB force field [37].

Long-range electrostatics with a cutoff of 10 Å were computed using the particle mesh Ewald (PME) method [39] and the same cutoff was applied to detect the van der Waals interactions. Initially, the systems were minimized for 10,000 steps. During the subsequent annealing, the Langevin thermostat was operated to control the temperature from 0 to 300 K at constant volume (NVT) for 200 ps. The SHAKE algorithm was employed to constrain all bonds involving hydrogen atoms [40]. For all systems, 50 ns simulation was executed at 300 K and 1 atm constant pressure (NPT). Trajectory snapshots were obtained every 2 fs.

2.3.1. Stability analysis of the auto-inhibitory catalytic-domain complex

Post simulation processing of all the trajectories of the aforementioned complexes was performed by employing the CPPTRAJ v17.00 module [41]. Basic root-mean-square deviation (RMSD), root-mean-square fluctuation (RMSF) and radius-of-gyration (Ro_g) analysis were calculated to evaluate the stability of the systems throughout the simulation. RMSD analysis was estimated for all backbone atoms of the complexes in which the starting structure was taken as a reference frame. Similarly, the residual fluctuation of backbone atoms was also calculated with RMSF analysis. In parallel, to evaluate whether the systems are steadily folded or not throughout the assigned simulations time, the radius of gyration (Ro_g) was also estimated for the selected complexes.

Graphical representations of the stability analysis plots given in the study were generated using Xmgrace [42].

2.3.2. Hydrogen-bond analysis

In order to understand the role of hydrogen-bonding in the folding of the inactive state of PKGIα, we analysed the occurrence of hydrogen-bonds between the AI domain and catalytic domain. Domain-domain as well as intra-domain interactions were also compared. Additionally, we compared the intra-domain hydrogen-bond analysis of auto-inhibitory bound PKGIα complexes with the apo-state of the catalytic domain to see the change of the hydrogen-bonding pattern between the auto-inhibitory bound and unbound states of the catalytic domain of PKGIα. We anticipate that there would be a few promising movements in the catalytic pocket of the PKGIα which help the AI domain to adjust with in the catalytic domain for blocking its activity. To that objective, MD trajectories of all complexes were subjected to CPPTRAJ module [41] to obtain a comprehensive hydrogen-bond analysis of AI2 and AI3 to explain different dynamic events attributed to hydrogen-bond occupancy.

2.3.3. Essential dynamics

Principal Component Analysis (PCA) [43] was also performed to understand the significant internal correlated structural transitions that take place within the catalytic domain to accommodate the AI domain. By utilizing MD trajectory data of AI2 and AI3, we identified and distinguished the secondary structure movement taking place within the AI domain-bound catalytic structures as compared to the apo-states. PCA uses structural transitions of the backbone-atoms matrix by removing overall rotational and translational movements to construct a covariance matrix [44]. Structurally uncorrelated variables known as 3 N eigenvectors (eigenvalues) are extracted from the diagonalization of the covariance matrix. Molecular dynamics simulation trajectories were then projected over these eigenvectors so defining the modes and amplitudes of the collective motions. These eigenvectors were calculated in descending order where the first principal component (PC-1) corresponds to the highest configurational space of the macromolecule. Eigenvectors of the two AI domain bound complexes and apo-system of PKGIα complexes were measured by applying CPPTRAJ. Close examination demonstrated that the first two eigenvalues constitute almost 80% of overall configurational space. Visual Molecular Dynamics (VMD) and Normal Mode Wizard (NMWiz) tools were employed to comprehensively investigate the uncorrelated system transitions and create porcupine plots respectively [45]. For graphical representations, PyMol and VMD were used [46,47].

2.4. Computational modelling of inactive and active state of PKGIα

Modelling of a multi-domain proteins where all the domains are placed in correct relative orientations is one of the challenging tasks of structural biology. Protein kinases are known to switch between two opposite conformations corresponding to the inactive and active states. Three-dimensional structural information of PKGIα, including the conformational heterogeneity at the structural level of these two states, is crucial to understand the regulation of cGMP signalling pathway. To that aim, we assembled already available structural data to define their native quaternary organization using a computational protein modelling and docking approach. Kim et al., 2016 [9] provided a hypothesized pictorial representation of putative quaternary packaging of the multi-domain structure of full-length PKGI in both active and inactive conformations; this has been used as a guide in the current study.

2.4.1. Inactive state homology modelling

Efforts to obtain a complete atomic structure of PKGI in any of the reported conformations have not yet been productive. Bakkouri et al., 2019 have recently reported experimentally solved crystal structures of PKG from *Plasmodium falciparum* and *Plasmodium vivax* in their inactive conformations [48]. Although there has been a pronounced divergence between *Plasmodium* and human cGMP kinase, it was the only available structural information demonstrating the folding behaviour of the tandem cGMP binding domains and C-terminal catalytic domain in PKG. To understand the tertiary architecture of inactive PKGIα, we applied comparative modelling using Modeller v 9.20 [49]. The amino acid sequence of PKGIα (UniProt ID: Q13976) was retrieved from UniProt and PSI-BLAST was performed against all the known structures in the protein databank (PDB). An appropriate template with reasonable percentage identity in maximum query coverage was selected. It was observed that the template structure is monomeric while literature reports that the human PKGIα exists in the homodimeric state. Crystal structures of leucine zipper domain (PDB Id: 4RL4) [50] and tandem cGMP binding domains (CNB-A and CNB-B) (PDB Id: 4Z07) [9] have clearly defined the residues responsible for the dimerization of PKGIα. Furthermore, domain orientation of the template was also compared with the orientation of inactive-state model of human PKGIα proposed by Kim et al., 2016. Only half of the structure was kept as template in which individual homologous domains are present in similar orientations to those proposed in the aforementioned study. Sequence-structure homology of template and query protein was also generated using Fugue [51], which identifies distant homologues and provides sequence-structure correlations of query proteins with known/solved homologous. It also provides 3D structural features of the protein sequence in a structure alignment. Modeller [9.22] was then used to build a single chain model [52]. The entire structure was used as a template primarily to ensure similar domain orientation while the local secondary structures of individual domains were kept intact by using solved structures of human PKGIβ CNB-A domain (PDB Id: 3OGJ_C) in apo-form, CNB-B domain (PDB Id: 4Z07) and catalytic domain (PDB Id: 6BDL) in apo-form as additional templates for modelling. Initially, the best model was selected based on DOPE score [53] and GA341 values [54]. Sister chains were submitted to ClusPro server for protein–protein docking and the best model was selected from all the clustered docked poses based on a similar inactive conformation to that proposed in the literature.

2.4.2. Active state homology modelling

To build an active-state model model of human PKGIα, AIDA (*ab initio* Domain Assembly) server [55] was used to assemble all the individually known and predicted domains together in a single chain. AIDA takes Protein Data Bank (PDB) files of individual domains as well as the amino acid sequence of the query protein to assemble all the consecutive domains. It uses PSI-Blast against the PDB to calculate position specific scoring matrix (PSSM) which was further employed to PSIPRED for calculating secondary structures and solvent accessibility. Based on the solvent accessibility analysis it keeps the predicted buried residues inside the core while the position of the domain which has high content of solvent assessable residues lies on the periphery to interact with the adjacent domain. Continuous domains are then assembled through a four-residue linker to attain a near native folded state. It returns the final assembled model at a lower/stable energy state through a built-in energy minimization protocol of AIDA. A full length assembled PKGIα subunit was selected based on its smaller RMSD value with the co-crystal structure of the tandem CNB (CNB-A/B) domains of human PKG I beta with cGMP (4Z07). As we lacked an entire length homologous template in dimeric form for our query protein, we applied protein–protein docking to decipher

the best appropriate orientation of our predicted homodimer. Both the AIDA predicted chains were submitted to DOCK module for protein–protein docking in ClusPro server [29]. From the advanced options, the multimeric docking option was applied with known distance restraints based on experimentally-known structures to get the best approximate homo-dimeric structure. The best docked dimeric model was them compared with CNB-A/B dimeric crystal structures to minimize the chance of predicting incorrect inter-chain interactions in the folded state.

Energy minimizations of both inactive and active models were performed in Schrödinger Release 2018 (Schrödinger Release 2018_4, LLC, New York, NY, 2018) by applying optimized potential for liquid simulations 2005 (OPLS 2005) force field [56]. The quality of the initial and refined inactive and active-state PKGIα models was estimated using RAMPAGE [57]. Maestro 11.8 (Schrödinger Release 2018-4: Maestro, Schrödinger, LLC, New York, NY, 2018) was used for surface and cartoon figure illustration.

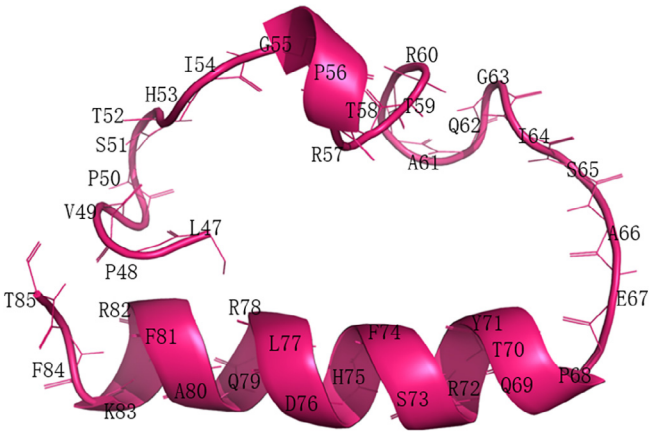

Fig. 2. Predicted model of AI domain of PKGIα.

3. Results

3.1. Homology modelling of the AI domain

From the top five predicted models, the best was selected based on TM and RMSD scores. The functionally important pseudo-substrate motif appears in the loop region and a long α-helix was observed in all the predicted models. It was anticipated that this N-terminal pseudo-substrate-motif-bearing region of the AI domain will be highly flexible, so allowing the substrate-like motif to engage with the catalytic domain. (shown in Fig. 2). The C-score indicates the significance of threading-template alignments and predicts a model based on the biological assembly of multiple sub-structures. Typically its score lies between −5 and 2. C-score of our predicted model of AI domain was −2.27 and TM score of 0.45 ± 0.14 Afterwards, the initial predicted model was further refined to adjust overall geometry and stereo-chemical clashes through energy minimization using MMF94s force field in UCSF Chimera [27,58].

3.2. Docking analysis of PKGIα auto-inhibitory domain & catalytic domain

Based on the different orientations of the docked AI domain within the PKGIα catalytic domain, our first docked conformer was denoted as AI1, the second as AI2 and the third as AI3. Initially a two-dimensional (2D) interaction analysis of these aforementioned docked poses was performed using Ligplot^{+} while a comprehensive three-dimensional (3D) interaction analysis elaborating all the intermolecular interactions, i.e. hydrogen-bond interactions, electrostatic interactions, van der Waals forces and hydrophobic interactions that stabilize the affinity of the AI domain to catalytic domain was done in Intermezzo. Ligplot^{+} results of three selected docked complexes are given in supplementary Fig. 1.

Docking analysis of the AI1 complex revealed a dock score of −870.1 kcal/mol while the AI domain was observed to engage the entry site of the catalytic pocket. In AI1 it was noted that the highly flexible N-terminal loop containing the pseudo-substrate motif is placed alongside where it is interacting more with the surface residues (Fig. 3a). Multiple hydrogen-bonds, polar interactions, ionic bonds and aromatic ring-ring interactions were observed between the residues of AI domain and catalytic pocket residues. Amongst the catalytic pocket residues, side chain atoms of H396, E523 and F371 were participating in hydrogen-bonding with the side chain atoms of S65, Q62 and Q79 respectively, while T400, Q402, E488, G520 and D657 were making polar interactions with the A66, P68, K83, Q79 and A61, respectively. In addition to these interactions, ionic-bond formation between R401 of the catalytic domain and E67 of the AI domain shown in Fig. 3d. Various π-π stacking interactions were also observed between catalytic domain residues, i.e. F505, W447, E488 and AI domain residues i.e. Y71, F74, L77 and R82. The orientation of AI domain in AI1 complex seems to interfere with the opening of the catalytic domain. In the AI1 complex, five residues, A61, Q62, I64, S65 and A66, of the seven residues of the pseudo-substrate motif (RAQGISA), were involved in various electrostatic interactions with the surface residues catalytic domain. The smallest number of hydrogen-bonds were observed in this complex.

Electrostatic interaction analysis of the AI2 complex revealed a dense network of interdomain interactions that mediate the binding of the AI domain within the catalytic cleft of PKGIα. In our second potent complex, the small helix was a little displaced from the active pocket while ClusPro dock score was −960.0 kcal/mol (Fig. 3b). In this complex, a small displacement of the AI domain's helix makes more room for the loop/unstructured part of the AI domain containing pseudo-substrate motif (RAQGISA) to interfere with the residues of the catalytic groove of the catalytic domain. Three-dimensional molecular interaction analysis using Intermezzo revealed fourteen hydrogen-bonds, eight van der Waals interactions, three polar interactions and seven hydrophobic and/or aromatic ring-ring interactions implicated in auto inhibition of the catalytic region of PKGIα. Residues of AI domain such as R60, A61, Q62, G63, I64, S65, A66, T70, Y71, R72, H75, L77 and F81 were making hydrogen-bonds of different strengths with D657, E658, N656, G369, G370, H396, E488, V368, R451, D650 and W447 of the catalytic residues. In the AI2 complex, all significant pseudo-substrate residues were participating through hydrogen-bonding with the catalytic domain. Furthermore, eight van der Waals interactions between R60, Q62, R78, Q79 and R82 residues of the AI domain and N655, D657, K393, G370, R451, D650 and S651 of the catalytic domain were fostering vital inter-domain contacts. In addition to these, polar interactions between Y71, P68 and S65 were also established with G370 and E445 of the catalytic region. Four hydrophobic interactions between catalytic residues i.e. F652, V638, R371, D657 and AI domain residues, i.e. F74 and Q62, were also evident in stabilizing the structural domain–domain interaction between PKGIα catalytic domain and AI domain (Fig, 3e). None of the critical catalytic residues was found interacting with the AI domain in the AI2 complex.

AI3, the third top ranked complex with plausible and/or potential inhibitory conformation with dock energy of −1666.0 kcal/mol, was further explored through interaction analysis tools (Fig. 3c). The highest number of hydrogen-bonds occurred in this docked complex as compared to the AI1 and AI2 complex. Catalytic

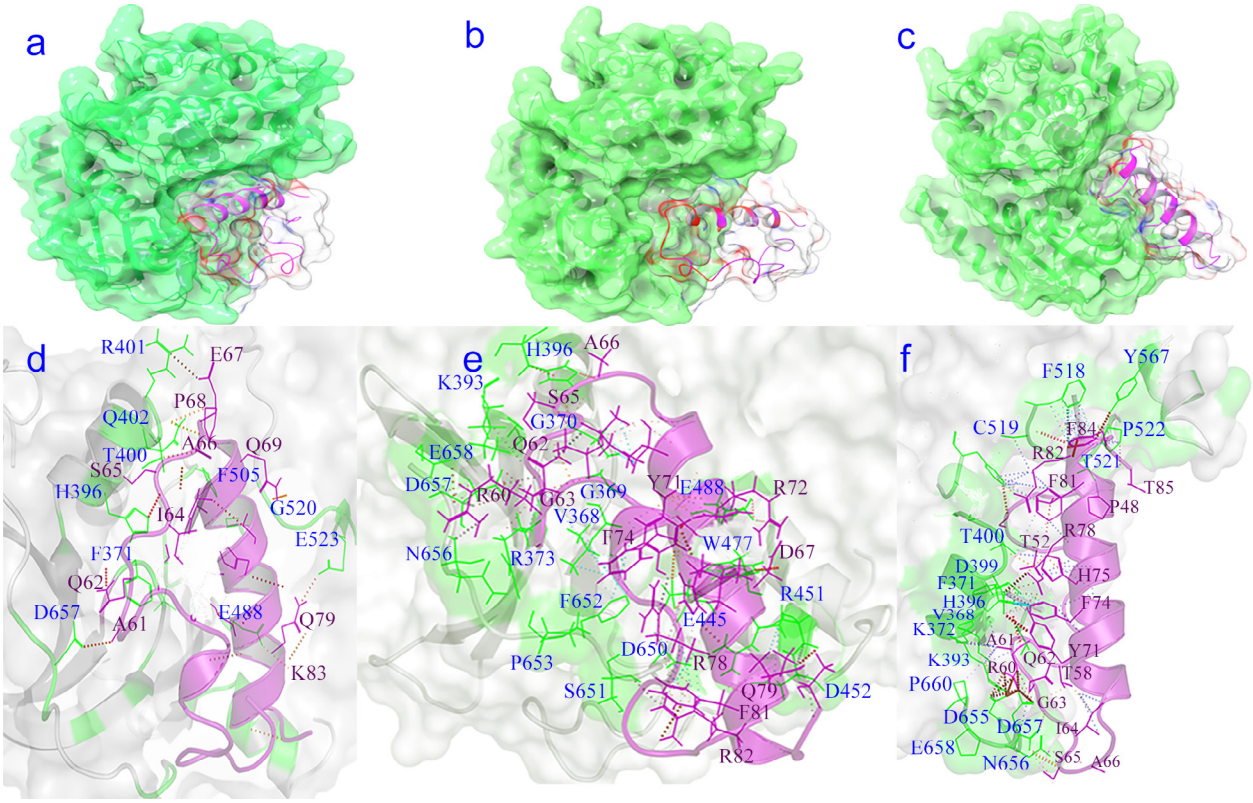

Fig. 3. Surface representation of three different docked conformations (AI1, AI2, AI3) (a, b, c) of N-terminal AI domain (purple) into the C-terminal catalytic domain (green) of PKGIα. (d, e, f) illustrate interaction diagrams of three conformers AI1, AI2, and AI3. Residues of the catalytic domain are labelled in blue and AI domain in black. Hydrogen-bonds are highlighted in red, polar interactions in orange, ionic bonds in brown, van der Waals interactions in grey, hydrophobic interactions in blue, carbonyl interactions in yellow and aromatic interactions in cyan. (For interpretation of the references to colour in this figure legend, the reader is referred to the web version of this article.)

domain residues i.e. F371, D657, D399, E658, F313, K393 and T399 are interacting with the R60, Q62, G63, I64, S65, A66 (RAQGISA), Y71, R78 motif by making hydrogen-bonds (Fig. 3f & Supplementary Fig. 1). In PKGIα, catalytic domain side chain atoms of D399, K393, T400, F505, C519, P522 and E658 were participating in the dense hydrophobic interactions, i.e. with F74, F81, R78, F84 and A61. Donor-π-interactions between the sidechain atoms of H396, F518 of the catalytic domain and F74 and F84 of the AI domain were also observed in AI3 complex (Fig. 3f).

In all the three selected complexes, AI2 and AI3 showed the binding of almost all the residues of pseudo-substrate motif with the catalytic domain residues. A smaller number of RAQGISA interactions were noted in the AI1 complex. From the docking interaction analysis, it was observed that in the complex AI3, three autophosphorylation sites T58, S65 and T85 of AI domain were occupied by D657, E658 and P522 respectively, through polar interactions (Supplementary Fig. 1). With the exception of the AI3 complex, both complexes lack these interactions. Studies reported the less rigid interactions of these autophosphorylation sites with the catalytic domain. From the docking analysis, we selected AI2 and AI3 for MD simulations.

3.3. Molecular dynamics simulations analysis

3.3.1. RMSD and Ro_g

The dynamics of the two best docked conformers (AI2 & AI3) were compared through all atom simulation using AMBER14 tools. To evaluate the conformational stability of our selected complexes, root mean square deviation (RMSD), root mean square fluctuation (RMSF) and radius of gyration (Ro_g) were investigated for all backbone atoms through CPPTRAJ.

Fig. 4 (upper panel) shows 50 ns RMSD trajectories of our top two ClusPro reported docked complexes of the AI domain with the catalytic domain. From the RMSD graph shown in Fig. 5, we observed that both AI domain-bound complexes are stable as compared to their apo-forms. No radical fluctuations in the peaks of AI2 and AI3 complexes were observed as compared to the apo-form. Selected complexes of AI and PKGI-α catalytic domain (denoted as AI2 and AI3) showed an average RMSD of 2.25 Å and 2.4 Å respectively (see Fig. 5). Whereas the apo system in which the AI domain is absent, showed an average RMSD of 2.25 Å till 30 ns, a sudden fluctuation to 4 Å was noticed at 35 ns which indicates a freely fluctuating pocket which otherwise accommodates ligand or pseudo-substrate motif in its inhibited state. After 35 ns, the apo-form again attained stability. Both AI domain-bound complexes showed a stable binding behaviour throughout the 50 ns simulation time. Our analysis revealed that binding of the AI domain to the catalytic domain confers stability to the docked systems by lowering its configurational space, possibly indicating the engagement of critical secondary structural elements of the catalytic pocket.

In addition to RMSD, the radius of gyration Ro_g was also investigated in the current study. Ro_g is an additional stability indicator that indicates the mass-weighted RMS distance of a cluster of atoms from their mean centre of mass; this provides a global dimension of the protein's mobility.

Ro_g analysis shown in Fig. 4 (lower panel) demonstrates that both selected AI domain-bound conformers of catalytic domain were found to be less variable throughout the simulation. Therefore, the overall values of Ro_g for AI2 and AI3 were approximately 20.4 Å, which signify moderate fold movement among all systems (Fig. 4). While the apo-form of the catalytic domain experiences a

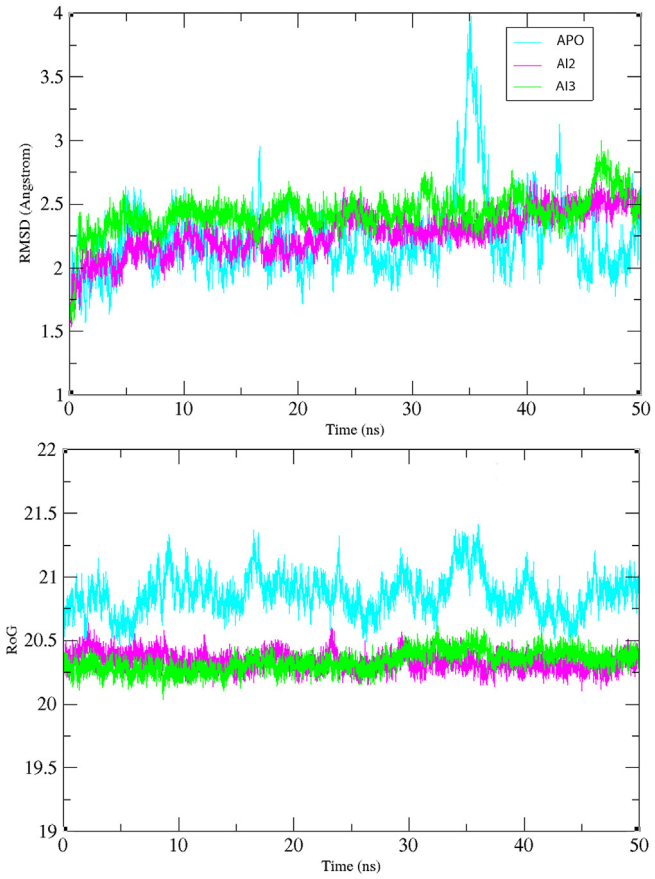

Fig. 4. Root mean square deviation (RMSD) and radius of gyration (Ro_g) graphs illustrating the stability of best-docked complexes of AI domain and the catalytic domain of PKGIα (AI2: purple; AI3: green) in comparison to the apo- form of the PKGIα catalytic domain (cyan). (For interpretation of the references to colour in this figure legend, the reader is referred to the web version of this article.)

large number of fluctuations that lie between 20.5 Å–21.25 Å, indicating the excitability of the ligand-free system. The results suggest that the structural fold of the catalytic domain when bound to the pseudo-substrate motif of the AI domain is actually contributing to the compactness of the AI2 and AI3 complexes over the course of the simulation. The Ro_g analysis results are in line with the RMSD stability analysis.

3.3.2. RMSF

In order to estimate the conformational flexibility of PRKGIα-catalytic domain upon binding the AI domain, RMSF was calculated for each system under study by considering the overall magnitude of fluctuation of each C_α-atom. Regions of the catalytic domain that anchor the AI domain in the AI2 and AI3 systems showed less fluctuation as compared to the apo-state. Within the catalytic pocket, the AI domain establishes electrostatic interactions with the residues present at β_1, L_2, L_3, α_2, L_4, α_3, L_5, β_5, L_7, β_6, α_4, α_6, α_7, L_{10}, L_{12}, L_{13}, α_9 and L_{20} regions of catalytic domain. During simulation, conformational changes in these important secondary structure elements were monitored. RMSF analysis of the catalytic domain revealed that in the apo-form β_1, L_2, L_3, α_2, L_{12}, L_{13} and α_9 showed an average 1.8 Å RMSF respectively, which indicates highly fluctuating regions (Fig. 5). Smaller amplitudes of displacements were observed at the aforementioned binding regions as all these attain stability after establishing interactions with the AI domain.

3.4. Hydrogen-Bond analysis

To focus more on the binding properties of the AI and catalytic domains, we analysed the hydrogen-bond propensity which corresponds to the interactions that occur persistently during the MD simulations. The hydrogen-bonds formed between AI2 and AI3 complexes with occupancy greater than 20% are enlisted in Table 1 and Table 2 respectively.

In the PKGIα AI2 complex, the contributing residues of the catalytic domain were located at the L_2, β_1, α_2, α_3,β_6, α_4, α_6, L_{12}, α_8, , L_{20} making protein–protein interactions with the **R60, A61, Q62, G63, S65, A66**, E67, Q69, Y71, R72, R78, Q79 and R82 of AI domain. In PKGIα catalytic domain, the side chains of E658: L_{12}, V368: β_1, G369, G370: $loop_2$, H396: α_2 were specifically interacting with **R60, A61, Q62, G63 and S65** residues of pseudo-substrate motif (RAQGISA). Interaction of the conserved glycine-rich β-hairpin loop residues i.e. G369, G370 and F371 with residues of the pseudo-substrate motif in the inhibited form are also reported in cAMP specific kinase (PKA). The pseudo-substrate motif not only stabilises the ATP-binding lobe of the catalytic domain but also stabilises the AGC kinase subdomain in the largest lobe by establishing hydrogen- bonds of remarkable occupancy. In the

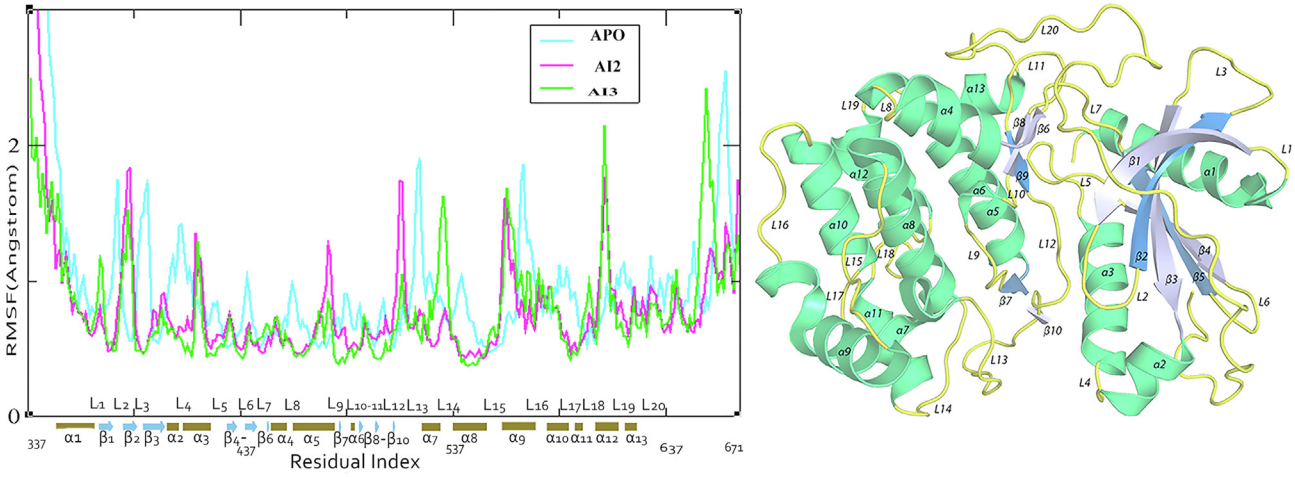

Fig. 5. Root mean square fluctuation (RMSF) analysis of the AI domain and catalytic domain conformers of PKGIα (AI2: purple; AI3: green) in comparison to the apo form of PKGIα catalytic domain (cyan). Secondary structure labelling of PKGIα catalytic domain (PDB Id: 6BDL). (For interpretation of the references to colour in this figure legend, the reader is referred to the web version of this article.)

Table 1
Comparison of hydrogen-bond interactions between binding modes AI2 and AI3 representing the docked conformations of AI domain and catalytic domain of PKGIα.

Auto-inhibitory-Catalytic Domain Complex	Acceptor	Donor	Percentage Occupancy	Average Distance	Average Angle
AI2	ASP_502@ O: $loop_{12}$	ARG_78@N	92.57	2.77	154.43
	GLY_370@O: $loop_2$	GLN_62@NE2	74.70	2.84	157.04
	ASP_399@H: α_2	GLU_67@OE1	73.66	2.84	156.28
	GLU_658@OE2: $loop_{20}$	ARG_60@NH1	72.78	2.79	158.60
	GLY_504@O: $loop_{12}$	TYR_71@N	71.62	2.76	161.95
	ASP_650@OD1: $loop_{20}$	ARG_82@NH2	63.90	2.81	158.26
	GLY_369@O: $loop_2$	GLN_62@NE2	60.08	2.84	158.48
	HIS_396@O: α_2	GLY_63@N	53.90	2.91	153.62
	VAL_368@O: β_1	GLN_62@NE	50.08	2.81	157.06
	GLU_488@OE1: $loop_8$	GLN_79@NE2	43.33	2.80	161.99
	ILE_406@O: α_3	ARG_60@N	42.33	2.83	159.35
	GLY_370@O: $loop_2$	SER_65@H	39.78	2.90	141.29
	GLU_445@OE1: α_6	TYR_71@OH	36.57	2.69	164.71
	GLU_488@OE1: $loop_8$	ARG_72@NH1	37.65	2.78	163.07
	GLU_402@OE1: α_2	ARG_602@NH1	35.09	2.79	158.53
	GLY_370@O: $loop_2$	ALA_61@H	33.67	2.91	145.84
	SER_651@O: $loop_{20}$	ARG_78@NH2	32.51	2.82	150.08
	ASP_657@OD2: $loop_{20}$	ARG_60@NE	29.37	2.76	174.89
	GLU_550@OE2: α_8	ARG_72@NH2	28.50	2.80	152.19
	THR_521@O: α_7	GLN_69@NE2	27.63	2.87	160.04
	GLU_445@OE2: α_6	ARG_82_NH1	23.70	2.85	147.42
	ASN_656_O: $loop_{20}$	ARG_60_NH2	22.46	2.87	157.50
	ASP_452_OD2: α_4	GLN_62_N	21.44	2.74	168.39
AI3	THR_521@O: α_7	ASP_76 @N	92.97	2.67	166.35
	ASP_399@OD2: α_2	GLN_62@NE2	73.66	2.84	156.28
	THR_521@OG1: α_7	VAL_49@N	62.10	2.91	150.68
	VAL_368@O: β_1	GLN_62@NE2	50.08	2.81	157.06
	ARG_401@O: $loop_4$	GLN_62@N	50.00	2.79	159.69
	HIS_396@O: α_2	GLY_63@N	47.30	2.62	153.62
	GLU_444@OE1: β_6	ARG_82@NH1	45.08	2.74	153.80
	LEU_366@O: β_1	ARG_82@N	36.93	2.82	148.53
	ASP_655@O: $loop_{20}$	ARG_60@NH2	36.59	2.78	161.38
	ASP_657@O: $loop_{20}$	ARG_60@NE	33.90	2.80	155.82
	PHE_371@OXT: $loop_2$	THR_52@OG1	33.46	2.85	142.76
	GLU_439@O: β_5	THR_52@N	32.09	2.89	154.16
	PHE_518@O:$loop_{13}$	GLN_69@NE2	32.37	2.79	155.21
	ASP_657@O: $loop_{20}$	ALA_61@H	30.02	2.89	163.45
	GLU_445@OE1: β_6	ARG_82@NH2	29.46	2.82	148.30
	GLY_370@O: $loop_2$	ALA_66@NH2	28.49	2.92	145.84
	VAL_368@O: β_2	ARG_78@NH1	28.50	2.86	146.46
	GLU_444@OE2: β_6	ARG_78@NE1	27.13	2.85	143.06
	LYS_393@O: β_3	GLN_62@N	31.76	2.85	162.62
	GLU_488@OE1: α_6	GLN_79@NE2	25.22	2.83	164.20
	GLU_488@OE2: α_6	LYS_83@N	25.62	2.73	160.13
	GLY_372@O: β_2	GLN_62@NE2	24.34	2.86	160.19
	ASP_502@OD1: $loop_{12}$	ARG_78@NH2	23.52	2.73	148.49
	ASN_656@OD1: $loop_{20}$	ARG_60@NH1	22.02	2.81	155.65
	GLU_658@O: $loop_{20}$	ARG_60@HE	22.55	2.80	156.96
	GLN_402@OE1: α_3	LYS_47@NZ	23.64	2.85	157.93
	GLY_370@O: $loop_2$	SER_65@OG	23.54	2.90	141.29
	HIS_396@O: α_2	SER_65@N	20.54	2.75	151.84
	GLY_369@O:$loop_2$	GLN_62@NE2	20.48	2.91	143.90

Table 2
Intradomain hydrogen-bond interactions in the apo-catalytic domain of PKGIα.

Catalytic Domain	Acceptor	Donor	Percentage Occupancy	Average Distance	Average Angle
APO	GLU_550@O: α_8	TYR_524@OH: α_7	91.89	2.72	163.73
	PHE_371@O: L_2	LYS_394@N: β_4	0.6928	2.86	164.47
	GLY_554@O: α_8	ARG_451@NH1: α_4	61.05	2.85	151.42
	GLU_439@OE1: L_7	ARG_423@NH1: L_5	46.50	2.88	149.91
	ASP_650@OD1: L_{20}	ARG_451@N: α_4	36.21	2.80	160.50
	ASP_502@OD2: L_{12}	ASN_489@N: α_6	32.03	2.86	158.53
	HIS_405@NE2: α_3	LYS_507@NZ: β_7	36.40	2.92	152.84
	ASP_502@OD1: L_{12}	TYR_482@N: L_{10}	30.24	2.75	156.23
	ASP_502@O: L_{12}	LYS_390@N: β_5	27.23	2.78	158.37
	GLU_445@O: β_6	VAL_368@N: β_6	27.010	2.91	156.98
	GLU_404@O: α_3	LYS_507@N: β_7	25.16	2.77	153.23
	PHE_371@OXT: L_2	LYS_393@N: β_3	23.54	2.86	158.17
	GLY_370@O: L_2	LYS_393@NZ: β_3	21.48	2.83	151.91
	GLY_369@O: L_2	HIS_396@N: α_2	21.00	2.82	158.77
	GLY_504@O: β_{10}	HIS_405@N: α_3	20.89	2.85	154.15

smaller lobe, potential interactions with the glycine-rich loop ($loop_2$) were observed while four residues S651, N656, D657 and E658 of the AGC kinase subdomain show high-affinity binding with the AI domain (Table 1). Ligand-interaction analysis using Ligplot$^+$ and hotspot analysis of the co-crystal structure of PKGI-α (PDB Id: 6C0T) revealed that four residues, F371: L_2 (glycine rich loop), E439: L_7, C441: L_7 and D502: L_{12} are critical catalytic residues that have a critical role in the activity of PKGIα. To understand the inhibitory potential of the binding mode of the AI domain in AI2 conformer, we noticed that D502:L_{12} forms a hydrogen-bond of 92.57% bond occupancy with R78 of the autoinhibitory region while none of the other critical catalytic residues were observed to be involved in interdomain hydrogen-bonding. Residues adjacent to F371, including V368, G369 and G370, keep the glycine-rich loop ($loop_2$) engaged in the interactions with residues of the pseudo-substrate motif over 50 ns simulation time.

To select the best configuration of the AI domain docked inside the catalytic domain, we analysed the hydrogen-bonding pattern of the AI3 complex, shown in Table 1. Hydrogen-bond analysis revealed that the AI domain binds through hydrogen-bonds of high occupancy throughout the 50 ns simulations with approximately twenty-four catalytic domain residues. Table 1 indicates the residues of the catalytic domain including L366, V368: β_1, G369, G370, F371: L_2, G372: β_2, K393: β_3, H396, D399:α_2, R401, Q402: L_4, E439: β_5, E445: β_6, E488: α_6, D502: L_{12}, F518: L_{13}, T521: α_8, D655, N656, D657, E568: L_{20} appear to form hydrogen-bonds with K47, V49, T53, **R60, A61, Q62, G63, S65, A66,** D76, R78, Q79, R82, K83. These hydrogen-bond interactions involve binding of the pseudo-substrate motif (RAQGISA) to the $loop_2$, commonly known as the glycine-rich loop, α_2, L_4, β_3, and L_{20}. These secondary structure regions cover the ATP-binding small lobe and the large lobe of the kinase subdomain as well as the AGC kinase domain, which is important for the function of the PKGIα catalytic domain. In complex AI3, it was also observed that all the critical catalytic residues, i.e. F371: L_2, D502: L_{12}, E439: β_5 except C441 are involved in accommodating the AI domain within the catalytic cleft with maximum hydrogen-bond occupancy. Based on the hydrogen-bond interaction analysis, the AI3 binding mode is considered to be the best possible configuration of the AI domain through which the pseudo-substrate motif blocks the activity of the PKGIα.

3.5. Motion mode analysis (PCA)

Following the hydrogen-bond analysis, essential dynamics associated with the concentrated eigenvectors of AI2, AI3 and apo form of PKGIα catalytic domain were extracted to explore the configurational space more precisely. The first and second eigenvectors (PC1&PC2) from the PCA analysis are presented in Fig. 6. The lengths of the porcupine quills represent the strength and degree of the motion while the heads of the arrows represent the direction of the motion. Principal component analysis (PCA) of AI3 showed potential movements within the small lobe and larger lobe of the catalytic domain. In apo-system α_1 showed significant flexibility that might help the C-terminal catalytic domain in coming closer to the AI domain located at the N-terminal in the inhibited state (Fig. 6a). After AI domain binding, L_4, which is present between α_3 and α_4, moves slightly outward to accommodate the AI domain. The AI domain helix moves inward to interact with residues located at L_{12} and L_{13}, which are lying at the junction of the small and large lobe of the catalytic domain and constitute the central deep groove of the catalytic pocket. L_{12} connects β_9 to β_{10} while L_{13} is connecting α_7 and β_{10}. Interaction of L_{12} and L_{13} residues with the autoinhibitory helix pulls α_7, β_9 and β_{10} of catalytic domain closer to the AI domain milieu. Furthermore, α_6 and α_9 also show a tendency of inward movement towards $loop_{13}$ and establish intradomain interactions that add more to the compactness of PKGIα catalytic domain. In comparison to the apo structure, there are few contacts between the AI domain and α_6 and α_9 helices of the catalytic domains of PKGIα that hold the pseudo-substrate motif and stabilize the closed/ inactive conformation. In the apo-structure, the opening of the catalytic pocket is a little wider compared to AI3 because α_9 helix in the apo-form is tilted away while in the AI3 complex α_9 helix tends to move inwards, which might indicate the entrapping of the AI domain between the small and large subdomains.

In the apo-state the restricted movement between the small and large lobes might be a consequence of a significant number of intradomain protein interactions. Specifically, the residues lying on α_3, α_4, α_6, α_7 and β_{10} are actively participating in the intradomain interactions with the residues of neighbouring secondary structures. Intradomain interactions in the apo system are shown in Table 2. While these aforementioned interactions are replaced by new interdomain protein–protein interactions in the AI-catalytic complexes (AI2, AI3).

The loop region of the AI domain carrying RAQGISA shows high flexibility and intrudes inside the catalytic pocket, establishing interactions with G444 and E445 of β_6 in the AI3 complex (Table 1). These particular interdomain interactions may influence secondary structure movements inside the binding pocket and help to bring β_5 and β_6 closer by introducing hydrogen-bond interactions between E439 (critical catalytic residue) and Thr52 of AI domain.

Unlike the AI3 complex, AI2 does not show significant secondary-structure transition in the catalytic domain after binding the AI domain. In Fig. 3 the AI domain lies slightly away from the binding pocket in AI2, while in AI3 it lies within the catalytic pocket where its highly flexible loop region tends to move inside the catalytic domain. The results from the hydrogen-bond interaction analysis and PCA analysis imply that AI3 is a more plausible binding mode that introduces convincing inter-domain interactions and undergoes significant conformational changes that are important to various aspects of the activity of the PKGIα in humans.

3.6. Dimer modelling

Our predicted homo-dimeric homology model of inactive PKGIα involves residues 103-671, which includes two consecutive cGMP binding domains and the C-terminal catalytic domain. While the cGMP-bound active-state homodimer is composed of 1-671 residues covering the N-terminal leucine-zipper domain, AI domain, four cGMP-binding domains (CNB-A, CNB-B) and a C-terminal catalytic domain.

Ramachandran analysis of the initial inactive model showed 83.2% of all residues in favoured while 93.7% of all residues were found in allowed regions. While the refined inactive model showed 91.8% of all residues in favoured regions, 7.8% and 0.4% of all residues were in allowed regions and outlier regions respectively demonstrating that the refined model is more stable than the initial one. In the active model, 93.2% of all residues are in favoured region, and 98.5% of all residues are in allowed regions after refinement. The RSMD difference of the final model with the crystal structure of the individual domains of human PKGIα is <0.8 Å RMSD. Orientations of all the adjacent domains in PKGIα inactive state model given in Fig. 7a & b are in agreement with the orientations of neighbouring domains proposed in inactive conformer of PKGIα by Kim et al., 2016.

Similarly, the best dimer model of the active chain of PKGIα was selected and validated through its superposition with the crystal structure of tandem CNB domains that are critical for active state dimerization (PDB Id: 4Z07), which showed an RMSD difference of 0.475 Å. The minimum RMSD score indicates that the full-length active-state model of PKGIα retained all the dimer contacts

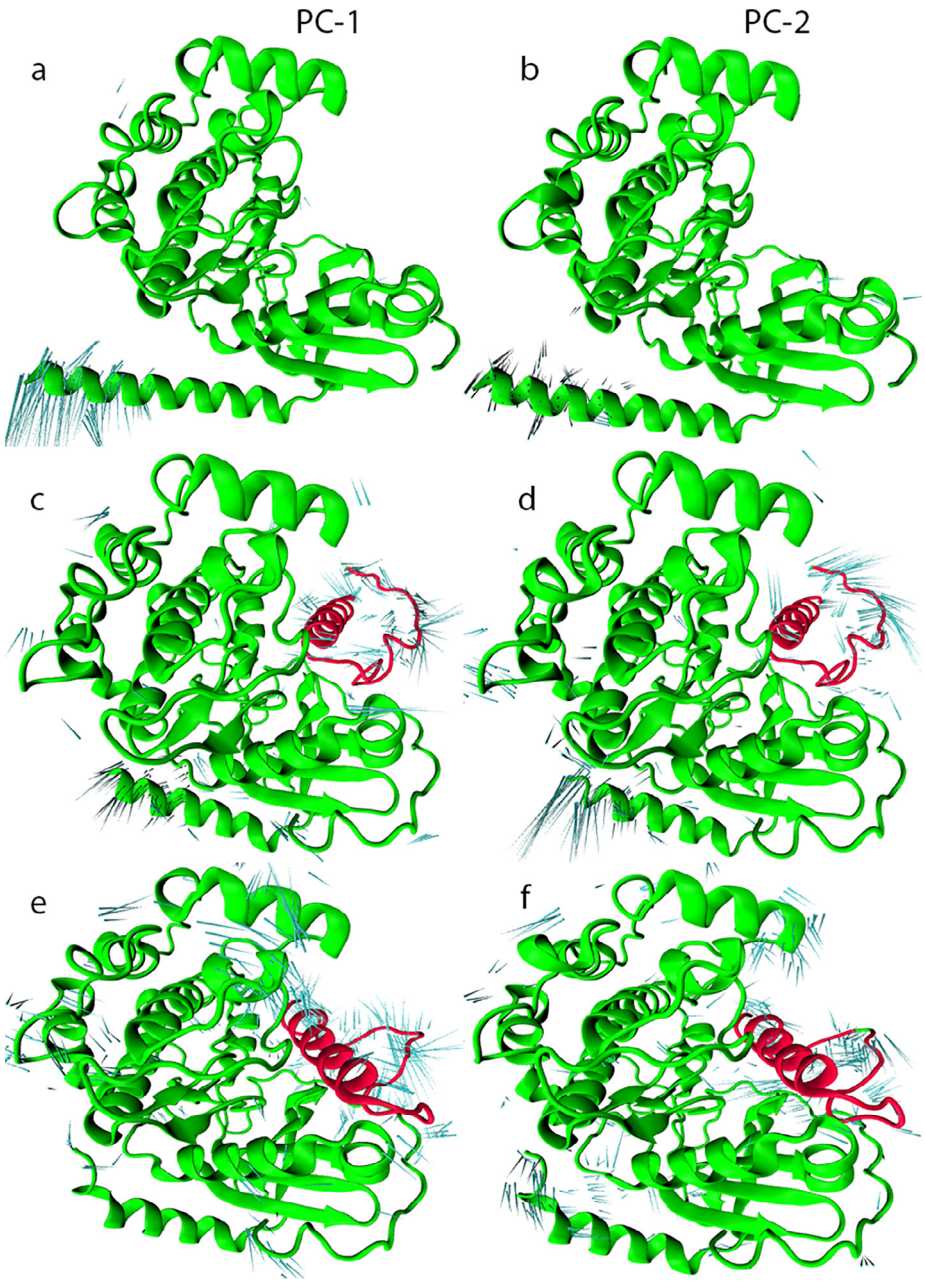

Fig. 6. The first two principal components (PC-1) and (PC-2) calculated for the apo-state of PKGIα catalytic domain (a, b) and the AI domain-bound complexes of PKGIα catalytic domain AI2 (c, d) and AI3 (e, f). The catalytic domain is shown in green colour and the AI domain is in red colour. The direction and magnitude of secondary structure movement is depicted in blue colour. (For interpretation of the references to colour in this figure legend, the reader is referred to the web version of this article.)

reported in experimental study. Overall the tertiary structure of the full-length active PKGIα is found consistent with the plausible domain orientation given in study by Kim et al., 2015 (Fig. 8A & B).

In the inactive state model shown in Fig. 7b, the long central helix that connects the two cGMP-binding domains in a single chain keeps them away from each other while in the active state, the central helix breaks and bends in the centre to bring cGMP binding tandem domains closer to each other. In the inactive state the cGMP binding domain A is coupled with the cGMP binding domain B of the sister chain (Fig. 8A & B). However, in the active model, cGMP domains of the two sister chains become uncoupled from each other (Fig. 7A & B).

In the PCA analysis of apo system, the N-terminal helix of the catalytic domain showed largescale movement (Fig. 6). Ligand induced conformational changes are communicated from the regulatory region of PKGIα to its catalytic region through this switch /N-terminal α_1 helix of catalytic domain. Previous studies reported the role of this helix in bringing a large conformational change from active sate to inactive state [12,33,59]. Movement of this helix might help the catalytic domain to bend over and entrap AI domain that is located at the N-terminal of PKGIα. Alongside, structural changes in the long central helix bridging CNB-A and CNB-B domains are also playing a key role in switching PKGIα in two different functional states [60]. In an inactive state, the sister chains in PKGIα homodimer are arranged antiparallel to each other. Long central helix bridging CNB-A and CNB-B domains extends due to the ligand uncoupling. A similar domain organization of tandem CNB-A and CNB-B domains and structural features of this central long helix were observed in the crystal structure of the regulatory subunit of PKAIIβ in *Mus musculus* (PDB Id: 4X6Q)

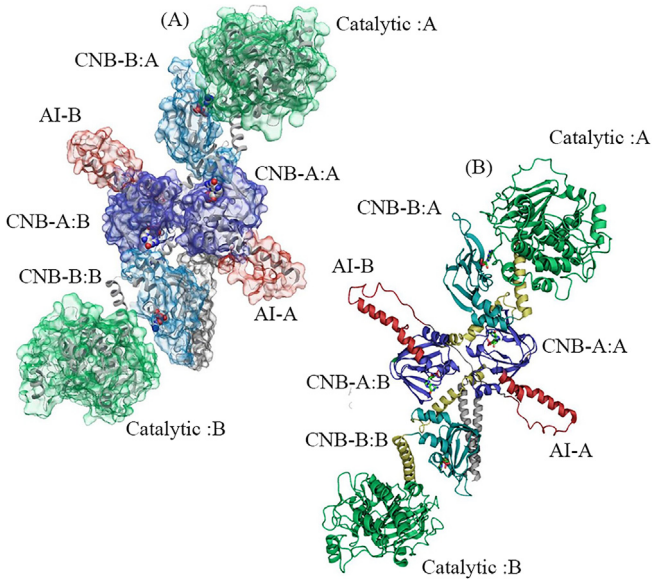

Fig. 7. Surface (A) and cartoon (B) representation of active-state model of full-length human (PKGIα) in complex with four cGMP molecules. Leucine zipper domains (LZ: grey), Auto-inhibitory domain (AI: red), cGMP binding domain A (CNB-A: blue), cGMP binding domain B (CNB-B: cyan) and catalytic domain (green). (For interpretation of the references to colour in this figure legend, the reader is referred to the web version of this article.)

[20]. In an elongated active conformation, this central helix is broken, this might allow the cGMP-binding domains to displace from their positions. In the inactive state, it was observed that CNB-A domain of the A chain is facing the CNB-B domain of the B-chain. Both these domains might be involved in dimerization but in the active state model, the CNB-A chain is facing the central helix of the B chain that connects the tandem domains. The regions between the tandem CNB domains of A and B chains and the cGMP molecules are involved in the dimerization of the two chains. It has been the reported that the rearrangement of the dimeric interaction is due to cGMP binding at CNBs domains that causes slight domain displacement in the active state [61,62]. Inter-domain interaction pattern of the tandem CNB-A and CNB-B as well as the local and global changes in their dynamics upon cGMP binding and cAMP binding in PKG and PKA, respectively are important for the elongation and activation of these homologous enzymes [63,64].

The adjustments of the CNB domains as a result of cGMP binding might bring a significant movement in the N-terminal helix of the catalytic domain to dislodge it from the AI domain. A distinct third state of PKGIβ also exists due to partial agonism of cyclic adenosine monophosphate (cAMP). cAMP induced dynamic changes in switch helix influence the relative orientation of regulatory and catalytic region of PKG [59].

4. Discussion

In this study, we explore the domain-domain interactions of AI and catalytic domains that govern the self-inhibitory mechanism of PKGIα using computational biophysical and *in silico* structure prediction methods. The inhibitory behaviour of AI and the catalytic domain is investigated in order to understand the molecular mechanism of autoinhibition of the PKGIα. In kinases, protein–protein interactions of two domains are often mediated by the presence of a regulatory motif that mimics the substrate and whose particular recognition sites are present on the partner domain [12]. Protein-protein interactions between specific binding partners at distinct recognition sites help the proteins to fold, assemble and evolve into complex molecular machines with specific functions [16,65]. Careful positioning of AI pseudo-substrate motif is critical for the proper functioning of the PKGIα.

To unravel the autoinhibitory mechanism of PKGIα, this study aims at understanding the nature of interactions involved in the inhibition of the catalytic activity. Although the nature of the residues in the pseudo-substrate motif of cyclic nucleotidyl protein kinases has been widely studied, less has been done regarding the structural aspects of the autoinhibition of the PKGIα. Protein docking, comprehensive interdomain-interactions analysis and MD simulation analysis provide evidence of the preferred conformer of the AI domain in the inactive state. Experimental studies have reported the role of catalytic residues (F371, E439, C441 and D502) that are lying at the glycine rich loop L_2, β_5 and L_{12} in the catalytic activity of the PKGIα [11,66]. It is also evident that pseudo-substrate motif RAQGISA is stabilising the positions of the residues of the glycine-rich loop and substrate-binding lobe [33]. Our findings with respect to the occupancy of critical catalytic

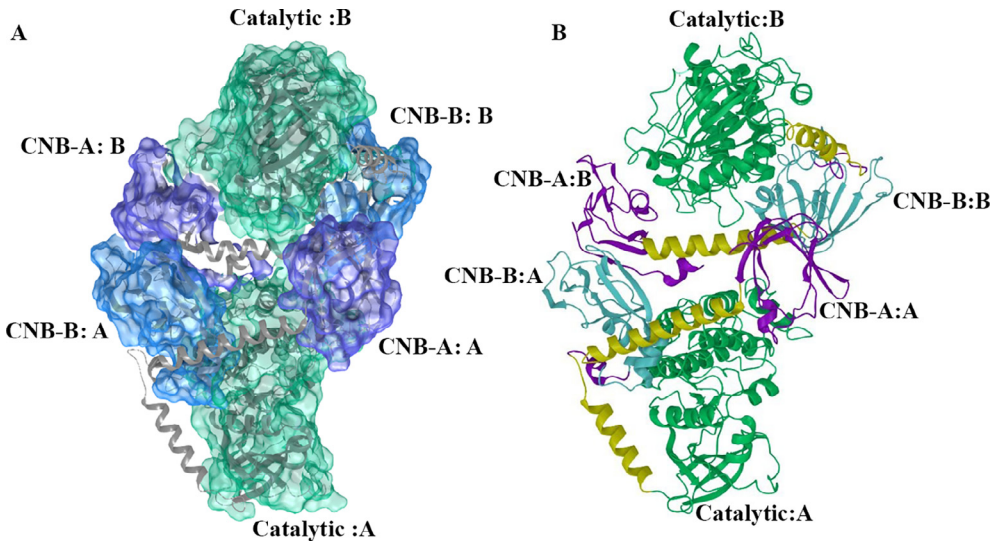

Fig. 8. Surface (A) and cartoon (B) representations of inactive-state model of full-length human (PKGIα). cGMP binding domain A(CNB-A: purple), cGMP binding domain B (CNB-B: cyan) and catalytic domain (green). (For interpretation of the references to colour in this figure legend, the reader is referred to the web version of this article.)

residues that cause the inhibition of the activity of catalytic domain are consistent with the experimental studies [66,67]. The presence of a helix in the AI domain that lies well inside the catalytic grove and the pseudo-substrate-motif-containing loop that snakes into the catalytic domain are also observed in the closely related PKA [68].

Docking interaction analysis identified polar interactions of catalytic residues i.e. D657, E658 and P522 with three of the four autophosphorylation sites i.e. T58, S65 and T85 of the AI domain. Among these residues, S65 has been reported to be significantly involved in increasing autoinhibition and decreasing cGMP binding affinity [10,13]. The region (611–658) present on the AGC kinase region of the C-terminal lobe is the conserved substrate-binding core of eukaryotic kinases [69]. In this study, three autophosphorylation sites of the AI domain are proposed to be engaged through polar interactions with the residues of the catalytic domain in the AI3 complex. Additionally, glutamate residues (observed in the AI3 complex) within the catalytic pocket are also considered as important residues that bind with the autoinhibitory pseudo-substrate motif that might block the activation of the PKGIα and retain it in the inhibited state. Several lines of evidence support the binding of the experimentally-reported auto-phosphorylation sites and pseudo-substrate motif of the AI domain through polar and hydrogen-bond interactions with the critical secondary structures of the small and large lobe of the catalytic domain in our selected complex [10,12,13,32,70].

It has been well established that human PKGIα exhibits different conformations in its active and inactive forms. Studies suggest that PKGIα experiences large conformational changes in order to switch from an inactive globular form to the catalytically active and elongated state. Large multiunit quaternary organization of the PKGIα apo- and holo-enzymes has been predicted in the current study by assembling all the available experimental and predicted structures. In the stable closed conformation, the catalytic domain folds over the central connecting helix of the cGMP binding domains (CNB-A & CNB-B) and the distance between α_1 helix of the catalytic domain and CNB-B decreases, probably inducing protein–protein interactions between them. These changes may allow the catalytic domain to come closer to the CNB-A domain and arrest the AI domain more easily as this domain is located at the N-terminal closer to CNB-A domain. In the closely related PKA, the linker harbouring inhibitory sequence helps stabilizing the inactive by disrupting its weak interactions with α-subdomain of the CNB-A domain which results in enhanced regulatory region and catalytic domain interface [64,71].

While in its active global structure, our results suggest that the α_1 helix of the catalytic domain has moved away from the CNB-B domain, which might have pushed the catalytic domain away from the CNB-A domain. Flexibility of the N-terminal α_1 helix of catalytic domain, as observed in the MD simulations of the apo-form and the AI-catalytic domain complexes, might help the PKGIα to switch between the compact ball-like folded inactive-state to an elongated active PKGI-α form. Our data also indicate high flexibility in the α_1 helix located the N-terminal of catalytic domain which connects the catalytic domain with the regulatory region of the PKGIα. A study by Huang *et al.* (2014) proposed large conformational changes in the N-terminal α_1 helix of the catalytic domain as well as in the central connecting helix of CNB domains (A and B) shown in supplementary Fig. 2 helps in lodging and dislodging of the regulatory region to/from the catalytic region [61 60,72]. Essential dynamics analysis highlighting the rigorous movement of this helix also underlined the highly dynamic nature the α_1 helix.

Past studies have reported a highly globular inactive state and a dumbbell-extended active-state conformation of PKGIα [9,73] This conformational change is due to the slight rearrangement of tandem cGMP-binding domains and their central connecting long α helix conformation that further dictates the α_1 helix of the catalytic domain to arrest or withdraw the AI domain. In switching from an open state to the closed state, role of dynamic linkers that are bridging different domain including central helix connecting CNB-A and CNB-B and N-terminal helix of the catalytic domain has been discussed above but modelling the loop/linker that connect the AI domain to the CNB-A domain was not successful in this study. Structural information of this particular dynamics linker is important in deciding the *cis* or *trans*- allosteric regulatory mechanism in PKGIα. Recently a study reported the *trans*-inhibition mechanism in PKGIβ in which the regulatory region of one PKG monomer binds the catalytic region of the other chain but we lack the experimental information yet [74].

Consistent with the already proposed observation, we conclude that the conformational dynamics is being driven by the protein–protein interactions between the PKGIα catalytic domain and the AI domain. The open and closed configurations of human PKGIα and structural details about the auto-inhibition mechanism, revealed in the present study, are although computationally-based but they provide strong basis for the proposed inner complex regulatory mechanism of human PKGIα in the cGMP signalling pathway.

Author contributions

A.R.S, A.M and T.L.B conceived and designed this study; A.M, S.C.V and S.S.C performed protein structure modelling. R.R.K performed MD simulations. A, M, S.C.V, A.E and R.R.K analysed all protein modelling and simulations results. A.M and R.R.K prepared the figures presented in the manuscript. A.M, R.R.K and S.C.V wrote first draft of the manuscript; T.L.B, A.E and A.R.S, improved and revised the manuscript. T.L.B provided overall support and guidance for the computational structure prediction. All the authors approved the final version.

CRediT authorship contribution statement

Arooma Maryam: Data curation, Formal analysis, Investigation, Methodology, Software, Validation, Visualization, Writing - original draft, Writing - review & editing. **Rana Rehan Khalid:** Data curation, Formal analysis, Investigation, Methodology, Software, Validation, Visualization, Writing - original draft, Writing - review & editing. **Sundeep Chaitanya Vedithi:** Investigation, Methodology, Software, Validation, Visualization, Writing - original draft. **Abdulilah ECE:** Methodology. Suleyman Selim Çınaroğlu: Methodology. **Abdul Rauf Siddiqi:** Conceptualization, Funding Acquisition, Methodology, Project Administration, Resources, Supervision, Writing-review and editing. **Tom L. Blundell:** Conceptualization, Funding Acquisition, Methodology, Project Administration, Resources, Supervision, Writing-review and editing. All the authors approved the final version

Declaration of Competing Interest

The authors declare that they have no known competing financial interests or personal relationships that could have appeared to influence the work reported in this paper.

Acknowledgment

A.M was supported by International Research Support Initiative Program (IRSIP) and National Research Program for Universities (NRPU: 4050) of the Higher Education Commission (HEC), Pakistan. A.M and R.R.K would also like to acknowledge 2216 Research Fel-

lowship Program for International Researchers by TUBITAK. S.C.V was supported by American leprosy Missions Grant (G88726), T. L.B was supported by the Wellcome Trust Investigator Award (200814/Z/16/Z).

Appendix A. Supplementary data

Supplementary data to this article can be found online at https://doi.org/10.1016/j.csbj.2020.06.016.

References

[1] Pfeifer A, Ruth P, Dostmann W, Sausbier M, Klatt P, Hofmann F. Structure and function of cGMP-dependent protein kinases. In: Reviews of physiology, biochemistry and pharmacology, vol. 135, Springer; 1999. p. 105–49.
[2] Hofmann F. The biology of cyclic GMP-dependent protein kinases. J Biol Chem 2005;280(1):1–4.
[3] Francis SH, Busch JL, Corbin JD. cGMP-dependent protein kinases and cGMP phosphodiesterases in nitric oxide and cGMP action. Pharmacol Rev 2010;62 (3):525–63.
[4] Beavo JA, Brunton LL. Cyclic nucleotide research — still expanding after half a century. Nat Rev Mol Cell Biol 2002;3:710.
[5] Edelman AM, Blumenthal DK, Krebs EG. Protein serine/threonine kinases. Annu Rev Biochem 1987;56(1):567–613.
[6] Busch JL, Bridges TM, Richie-Jannetta R, Hollett BP, Francis SH, Corbin JD. Catalytic site amino acids of PKGI-alpha influence allosteric cGMP binding. Front Biosci (Scholar ed) 2013;5:650–60.
[7] Qin L, Sankaran B, Aminzai S, Casteel D, Kim C. Structural basis for selective inhibition of human PKG Iα by the balanol-like compound N46. J Biol Chem 2018:jbc. RA118. 002427.
[8] Richie-Jannetta R, Francis SH, Corbin JD. Dimerization of cGMP-dependent protein kinase Iβ is mediated by an extensive amino-terminal leucine zipper motif, and dimerization modulates enzyme function. J Biol Chem 2003;278 (50):50070–9.
[9] Kim JJ, Lorenz R, Arold ST, Reger AS, Sankaran B, Casteel DE, et al. Crystal structure of PKG I:cGMP complex reveals a cGMP-mediated dimeric interface that facilitates cGMP-induced activation. Structure 2016;24(5):710–20.
[10] Moon TM, Sheehe JL, Nukareddy P, Nausch LW, Wohlfahrt J, Matthews DE, et al. An N-terminally truncated form of cyclic GMP–dependent protein kinase Iα (PKG Iα) is monomeric and autoinhibited and provides a model for activation. J Biol Chem 2018;293(21):7916–29.
[11] Alverdi V, Mazon H, Versluis C, Hemrika W, Esposito G, van den Heuvel R, et al. cGMP-binding prepares PKG for substrate binding by disclosing the C-terminal domain. J Mol Biol 2008;375(5):1380–93.
[12] Haushalter KJ, Casteel DE, Raffeiner A, Stefan E, Patel HH, Taylor SS. Phosphorylation of protein kinase A (PKA) regulatory subunit riα by protein kinase G (PKG) primes pka for catalytic activity in cells. J Biol Chem 2018;293 (12):4411–21.
[13] Busch JL, Bessay EP, Francis SH, Corbin JD. A conserved serine juxtaposed to the pseudosubstrate site of type I cGMP-dependent protein kinase contributes strongly to autoinhibition and lower cGMP affinity. J Biol Chem 2002;277 (37):34048–54.
[14] Lohmann SM, Walter U. Tracking functions of cGMP-dependent protein kinases (cGK). Front Biosci. 2005;10(518):1313–28.
[15] Kim C, Xuong N-H, Taylor SS. Crystal structure of a complex between the catalytic and regulatory (RIα) subunits of PKA. Science 2005;307(5710):690–6.
[16] Vogel C, Bashton M, Kerrison ND, Chothia C, Teichmann SA. Structure, function and evolution of multidomain proteins. Curr Opin Struct Biol 2004;14 (2):208–16.
[17] Khalid RR, Maryam A, Fadouloglou VE, Siddiqi AR, Zhang Y. Cryo-EM density map fitting driven in-silico structure of human soluble guanylate cyclase (hsGC) reveals functional aspects of inter-domain cross talk upon NO binding. J Mol Graph Model 2019;90:109–19.
[18] Maryam A, Vedithi SC, Khalid RR, Alsulami AF, Torres PHM, Siddiqi AR, et al. The molecular organization of human cGMP specific phosphodiesterase 6 (PDE6): structural implications of somatic mutations in cancer and retinitis pigmentosa. Comput Struct Biotechnol J 2019;17:378–89.
[19] Khalid RR, Siddiqi AR, Mylonas E, Maryam A, Kokkinidis M. Dynamic characterization of the human heme nitric oxide/oxygen (HNOX) domain under the influence of diatomic gaseous ligands. Int J Mol Sci 2019;20(3):698.
[20] Zhang P, Ye F, Bastidas AC, Kornev AP, Wu J, Ginsberg MH, et al. An Isoform-specific myristylation switch targets type II PKA holoenzymes to membranes. Structure (London, England : 1993) 2015;23(9):1563–72.
[21] Consortium U. UniProt: a hub for protein information. Nucleic Acids Res 2014;43(1):D204–12.
[22] Mount DW. Using the basic local alignment search tool (BLAST). Cold Spring Harbor Protocols. 2007;2007(7):pdb. top17.
[23] Er M, Abounakhla AM, Tahtaci H, Bawah AH, Çınaroğlu SS, Onaran A, et al. An integrated approach towards the development of novel antifungal agents containing thiadiazole: synthesis and a combined similarity search, homology modelling, molecular dynamics and molecular docking study. Chem Cent J 2018;12(1):121.
[24] Yang J, Yan R, Roy A, Xu D, Poisson J, Zhang Y. The I-TASSER Suite: protein structure and function prediction. Nat Methods 2015;12(1):7.
[25] Zhang Y, Skolnick J. TM-align: a protein structure alignment algorithm based on the TM-score. Nucleic Acids Res 2005;33(7):2302–9.
[26] Yang J, Zhang Y. Protein structure and function prediction using I-TASSER. Curr Protocols Bioinform 2015;52(1):5.8. 1–5.8. 15
[27] Pettersen EF, Goddard TD, Huang CC, Couch GS, Greenblatt DM, Meng EC, et al. UCSF Chimera—a visualization system for exploratory research and analysis. J Comput Chem 2004;25(13):1605–12.
[28] Davis IW, Murray LW, Richardson JS, Richardson DC. MOLPROBITY: structure validation and all-atom contact analysis for nucleic acids and their complexes. Nucleic Acids Res 2004;32(suppl_2):W615–W9
[29] Comeau SR, Gatchell DW, Vajda S, Camacho CJ. ClusPro: a fully automated algorithm for protein–protein docking. Nucleic Acids Res 2004;32(suppl_2): W96–W9.
[30] Tovchigrechko A, Vakser IA. GRAMM-X public web server for protein–protein docking. Nucleic Acids Res 2006;34(suppl_2):W310–W4.
[31] Cheng TMK, Blundell TL, Fernandez-Recio J. pyDock: electrostatics and desolvation for effective scoring of rigid-body protein–protein docking. Proteins Struct Funct Bioinf 2007;68(2):503–15.
[32] Yuasa K, Michibata H, Omori K, Yanaka N. Identification of a conserved residue responsible for the autoinhibition of cGMP-dependent protein kinase Iα and β. FEBS Lett 2000;466(1):175–8.
[33] Francis SH, Poteet-Smith C, Busch JL, Richie-Jannetta R, Corbin JD. Mechanisms of autoinhibition in cyclic nucleotide-dependent protein kinases. Front Biosci. 2002;7:d580–92.
[34] Yuan S, Chan HS, Hu Z. Using PyMOL as a platform for computational drug design. Wiley Interdisc Rev Comput Mol Sci 2017;7(2):e1298.
[35] Radoux CJ, Olsson TS, Pitt WR, Groom CR, Blundell TL. Identifying interactions that determine fragment binding at protein hotspots. J Med Chem 2016;59 (9):4314–25.
[36] Case DA, Cheatham III TE, Darden T, Gohlke H, Luo R, Merz Jr KM, et al. The Amber biomolecular simulation programs. J Comput Chem 2005;26 (16):1668–88.
[37] Maier JA, Martinez C, Kasavajhala K, Wickstrom L, Hauser KE, Simmerling C. ff14SB: improving the accuracy of protein side chain and backbone parameters from ff99SB. J Chem Theory Comput 2015;11(8):3696–713.
[38] Price DJ, Brooks III CL. A modified TIP3P water potential for simulation with Ewald summation. J Chem Phys 2004;121(20):10096–103.
[39] Darden T, York D, Pedersen L. Particle mesh Ewald: an N· log (N) method for Ewald sums in large systems. J Chem Phys 1993;98(12):10089–92.
[40] Kräutler V, Van Gunsteren WF, Hünenberger PH. A fast SHAKE algorithm to solve distance constraint equations for small molecules in molecular dynamics simulations. J Comput Chem 2001;22(5):501–8.
[41] Roe DR, Cheatham TE. PTRAJ and CPPTRAJ: software for processing and analysis of molecular dynamics trajectory data. J Chem Theory Comput 2013;9 (7):3084–95.
[42] Turner P. XMGRACE, Version 5.1. 19. Center for Coastal and Land-Margin Research, Oregon Graduate Institute of Science and Technology, Beaverton, OR; 2005.
[43] Ringnér M. What is principal component analysis?. Nat Biotechnol 2008;26 (3):303.
[44] Aalten DMFV, Findlay JBC, Amadei A, Berendsen HJC. Essential dynamics of the cellular retinol-binding protein evidence for ligand-induced conformational changes. Protein Eng Des Sel 1995;8(11):1129–35.
[45] Bakan A, Meireles LM, Bahar I. ProDy: protein dynamics inferred from theory and experiments. Bioinformatics 2011;27(11):1575–7.
[46] DeLano WL. The PyMOL molecular graphics system. San Carlos, CA, USA: DeLano Scientific; 2002.
[47] Humphrey W, Dalke A, Schulten K. VMD: visual molecular dynamics. J Mol Graph 1996;14(1):33–8.
[48] El Bakkouri M, Kouidmi I, Wernimont AK, Amani M, Hutchinson A, Loppnau P, et al. Structures of the cGMP-dependent protein kinase in malaria parasites reveal a unique structural relay mechanism for activation. Proc Natl Acad Sci 2019:201905558.
[49] Šali A, Potterton L, Yuan F, van Vlijmen H, Karplus M. Evaluation of comparative protein modeling by MODELLER. Proteins Struct Funct Bioinf 1995;23(3):318–26.
[50] Qin L, Reger AS, Guo E, Yang MP, Zwart P, Casteel DE, et al. Structures of cGMP-dependent protein kinase (PKG) Ialpha leucine zippers reveal an interchain disulfide bond important for dimer stability. Biochemistry 2015;54 (29):4419–22.
[51] Mizuguchi K, Deane CM, Blundell TL, Johnson MS, Overington JP. JOY: protein sequence-structure representation and analysis. Bioinformatics (Oxford, England) 1998;14(7):617–23.
[52] Burke DF, Deane CM, Nagarajaram HA, Campillo N, Martin-Martinez M, Mendes J, et al. An iterative structure-assisted approach to sequence alignment and comparative modeling. Prot Struct Func Bioinform 1999;37 (S3):55–60
[53] My Shen, Sali A. Statistical potential for assessment and prediction of protein structures. Protein Sci 2006;15(11):2507–24.
[54] Eswar N, Eramian D, Webb B, Shen M-Y, Sali A. Protein structure modeling with MODELLER, Structural proteomics. Springer; 2008. p. 145–59.
[55] Xu D, Jaroszewski L, Li Z, Godzik A. AIDA: ab initio domain assembly server. Nucleic Acids Res 2014;42(W1):W308–W13.

[56] Jorgensen WL, Tirado-Rives J. The OPLS [optimized potentials for liquid simulations] potential functions for proteins, energy minimizations for crystals of cyclic peptides and crambin. J Am Chem Soc 1988;110(6):1657–66.
[57] Lovell SC, Davis IW, Arendall III WB, De Bakker PI, Word JM, Prisant MG, et al. Structure validation by Cα geometry: ϕ, ψ and Cβ deviation. Proteins Struct Funct Bioinf 2003;50(3):437–50.
[58] Halgren T, Nachbar R, editors. MMF94: The Merck molecular force field. Bridging the gap-From small organics to proteins. Abstracts of papers of the American Chemical Society; AMER CHEMICAL SOC 1155 16TH ST 1996 NW WASHINGTON, DC 20036.
[59] VanSchouwen B, Selvaratnam R, Giri R, Lorenz R, Herberg FW, Kim C, et al. Mechanism of cAMP partial agonism in protein kinase G (PKG). J Biol Chem 2015;290(48):28631–41.
[60] Osborne BW, Wu J, McFarland CJ, Nickl CK, Sankaran B, Casteel DE, et al. Crystal structure of cGMP-dependent protein kinase reveals novel site of interchain communication. Structure (London, England: 1993) 2011;19 (9):1317–27.
[61] Huang GY, Kim JJ, Reger AS, Lorenz R, Moon E-W, Zhao C, et al. Structural basis for cyclic-nucleotide selectivity and cGMP-selective activation of PKG I. Structure 2014;22(1):116–24.
[62] Kim JJ, Lorenz R, Arold ST, Reger AS, Sankaran B, Casteel DE, et al. Crystal structure of PKG I: cGMP complex reveals a cGMP-mediated dimeric interface that facilitates cGMP-induced activation. Structure 2016;24(5):710–20.
[63] McNicholl ET, Das R, SilDas S, Taylor SS, Melacini G. Communication between tandem cAMP binding domains in the regulatory subunit of protein kinase A-Iα as revealed by domain-silencing mutations. J Biol Chem 2010;285 (20):15523–37.
[64] Akimoto M, McNicholl ET, Ramkissoon A, Moleschi K, Taylor SS, Melacini G. Mapping the free energy landscape of PKA inhibition and activation: a double-conformational selection model for the tandem cAMP-binding domains of PKA RIα. PLoS Biol 2015;13(11).
[65] Schillinger C, Boisguerin P, Krause G. Domain interaction footprint: a multi-classification approach to predict domain–peptide interactions. Bioinformatics 2009;25(13):1632–9.
[66] Qin L, Sankaran B, Aminzai S, Casteel DE, Kim C. Structural basis for selective inhibition of human PKG Iα by the balanol-like compound N46. J Biol Chem 2018;293(28):10985–92.
[67] Kalyanaraman H, Zhuang S, Pilz RB, Casteel DE. The activity of cGMP-dependent protein kinase Iα is not directly regulated by oxidation-induced disulfide formation at cysteine 43. J Biol Chem 2017;292(20):8262–8.
[68] Knighton DR, Zheng J, Ten Eyck LF, Ashford VA, Xuong N-H, Taylor SS, et al. Crystal structure of the catalytic subunit of cyclic adenosine monophosphate-dependent protein kinase. Science 1991;253(5018):407–14.
[69] Zhang P, Ye F, Bastidas AC, Kornev AP, Wu J, Ginsberg MH, et al. An isoform-specific myristylation switch targets type II PKA holoenzymes to membranes. Structure 2015;23(9):1563–72.
[70] Schlossmann J, Desch M. cGK substrates. cGMP: generators, effectors and therapeutic implications. Springer; 2009. p. 163–93.
[71] Akimoto M, Selvaratnam R, McNicholl ET, Verma G, Taylor SS, Melacini G. Signaling through dynamic linkers as revealed by PKA. Proc Natl Acad Sci 2013;110(35):14231–6.
[72] Moon TM, Osborne BW. Dostmann WR. The switch helix: a putative combinatorial relay for interprotomer communication in cGMP-dependent protein kinase. Biochimica et Biophysica Acta (BBA)-Prot Proteom 2013;1834 (7):1346–51.
[73] Dostmann WR, Koep N, Endres R. The catalytic domain of the cGMP-dependent protein kinase lalpha modulates the cGMP-binding characteristics of its regulatory domain. FEBS Lett. 1996;398(2–3):206–10.
[74] Kim C, Sharma R, Casteel DE. Correction to: crystal structure of PKG Iβ holoenzyme reveals a trans-inhibiting dimer assembly. J Transl Med 2020;18 (1):1–2.